Chemistry–A European Journal
Research Article
doi.org/10.1002/chem.202403108
Chemistry Europe
European Chemical Societies Publishing
www.chemeurj.org

Syn vs. Anti? What Controls Addition Stereochemistry in Chlorolactonization

Emily R. Dzurka Camelio,[b] Mitchell Maday,[a] Aritra Sarkar,[a] James E. Jackson,*[a] and Babak Borhan*[a]

The stereochemistry of the uncatalyzed chlorolactonization of 4-phenylpent-4-enoic acid at room temperature was examined to probe the reaction's intrinsic diastereoselectivities as a function of chlorenium ion donor, solvent polarity, and reactant concentration ranges. Kinetic studies using Variable Time Normalization Analysis (VTNA) revealed differing reaction orders for the *syn* and *anti* alkene addition processes. Aided and illustrated by quantum chemical modeling, this detailed mechanistic analysis of the substrate's intrinsic chlorolactonization reactions points to concerted Ad_E3-type paths for both *syn* and *anti* additions. By illuminating the factors selecting for *syn*- vs *anti*-addition paths, the results provide key reference points for future studies of stereocontrol in halofunctionalization reactions.

Introduction

Halofunctionalization has become a widely used and studied transformation in organic synthesis. This strategy has seen great progress over the years, in part due to its ability to efficiently construct molecular frameworks through catalytic asymmetric halofunctionalization.[1] Previous reports by our own and other groups have showcased this versatile tool's utility in providing access to a myriad of different scaffolds; one example is shown in Figure 1a, where deuterated **1-D** is exposed to catalytic chlorocyclization conditions to form **2-D**.[2]

The most common textbook mechanism for halocyclization reactions is stepwise, beginning with electrophilic halenium ion attack to form a bridged haliranium ion. Ring closure then occurs in a second step via S_N2-type attack on this halonium ion, resulting in net *anti* addition (Figure 1b). If one of the alkene termini is functionalized such that it forms an open carbocation, trapping by the internal nucleophile may occur on either face, yielding stereochemically scrambled chlorolactone products. Our own recent work has noted that halofunctionalization reaction rates are correlated to the nucleophilicity of the internal nucleophile proximal to the alkene (Figure 1c), providing evidence that these rate-limiting additions involve both the electrophilic and the nucleophilic partners. Here, the ability of the intramolecular nucleophile to activate the alkene π system for attack on the electrophilic halogenating agent points to a concerted Ad_E3-type addition mechanism. This "nucleophile assisted alkene activation" (NAAA) pathway has emerged as an important alternative to the more familiar stepwise processes,

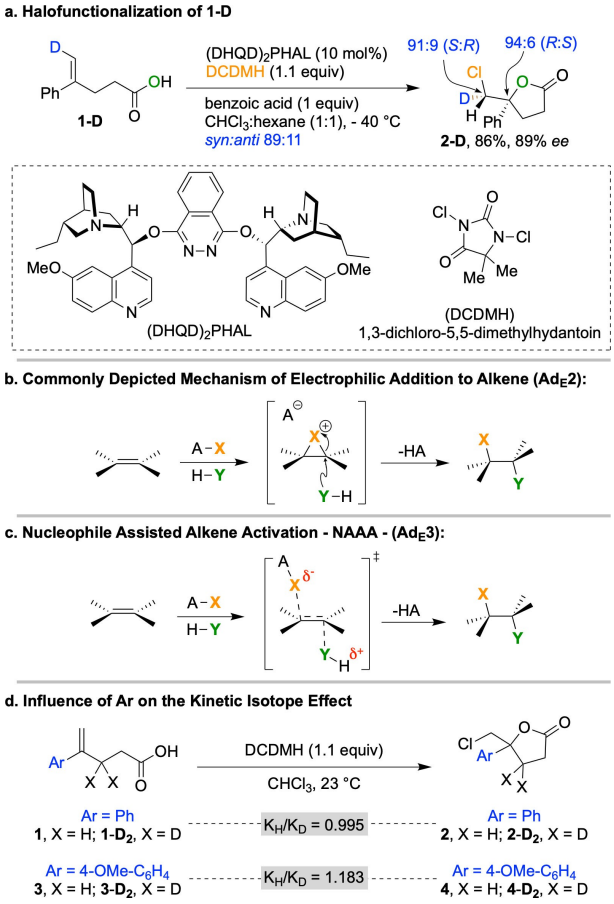

Figure 1. (a) Catalyzed chlorocyclization of **1-D**; (b) Classical depiction of electrophilic halogenation; (c) Concerted addition pathway for halogenation of an alkene; (d) secondary KIE for halolactonization of **1** and **3**.

[a] *M. Maday, A. Sarkar, J. E. Jackson, B. Borhan*
Department of Chemistry, Michigan State University, 578 S. Shaw Rd, East Lansing, MI 48824, USA
E-mail: jackson@chemistry.msu.edu
babak@chemistry.msu.edu

[b] *E. R. Dzurka Camelio*
Department of Green Chemistry and Biochemistry, University of Michigan-Flint, Flint, MI 48502, USA

Supporting information for this article is available on the WWW under https://doi.org/10.1002/chem.202403108

© 2024 The Author(s). Chemistry - A European Journal published by Wiley-VCH GmbH. This is an open access article under the terms of the Creative Commons Attribution License, which permits use, distribution and reproduction in any medium, provided the original work is properly cited.

© 2024 The Author(s). Chemistry - A European Journal published by Wiley-VCH GmbH

offering new possibilities for stereochemical control. In the case of chlorocyclization of **1**, additional evidence that an intermediate cation is avoided arose from the absence of an isotope effect due to deuteration at the methylene neighboring the benzylic site, in contrast to an example where the potential carbocation site was stabilized enough to be favored (Figure 1d).[3]

Using deuterium labeling to differentiate stereochemistry at the newly formed sp^3 center, CDHCl, the absolute and relative facial selectivity of chlorine (electrophile) and oxygen (nucleophile) addition across the double bond was revealed (Figure 1a). Here, the $(DHQD)_2PHAL$-catalyzed reaction of the deuterated carboxylic acid provided primarily *syn*-selectivity with a *syn*:*anti* ratio of 89:11, obviating mechanisms involving an *anti*-directing bridging 3-membered cyclic halirenium ion.[4] More recent mechanistic studies from our lab explored how the catalyst binds the substrate and templates the enantioselective ring closure through hydrogen bonding and van der Waals interactions, limiting the substrate's conformations to favor NAAA.[5] However, much less attention has been given to understanding the intrinsic nature and stereopreferences of these reactions in the absence of a catalyst. A full understanding of the reaction path and its stereochemical control elements is an essential reference point for the design and analysis of stereocontrolled alkene halofunctionalization reactions.

Results and Discussion

The goal of the present study is to understand the intrinsic diastereoselectivities of the uncatalyzed chlorocyclization of carboxylic acid **1-D**. Catalyzed by $(DHQD)_2PHAL$, this reaction strongly favors the *syn* product.[2a,4,5] However, the uncatalyzed chlorolactonization occurs sluggishly to provide a 34:66 *syn:anti* product ratio (Scheme 1). Significant *syn*-isomer formation suggests more than one path; if reaction proceeded via a cyclic chloriranium ion, only the *anti*-isomer would be expected.

Halenium Affinity (*HalA*) is a parameter that measures the strength of a Lewis base species' binding to a halenium ion. Comparing alkenes (or other Lewis bases), those with the greater *HalA* value are predicted to more readily capture the halenium ion. For the chlorolactonization reaction, it was found that the alkene precursor has the largest *HalA* value when in a conformation with the carboxylic acid (nucleophile) positioned near the alkene π system, poised for simultaneous attack on the olefin as it captures the halenium ion (Figure 2a). Though slightly above the lowest energy geometry, this conformation

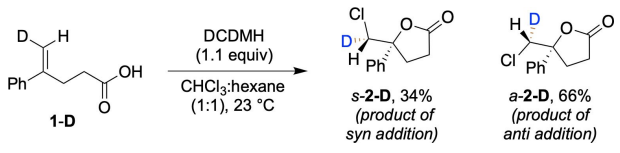

Scheme 1. Uncatalyzed chlorocyclization of **1-D** to give *syn* and *anti*-product (enantiomers not shown).

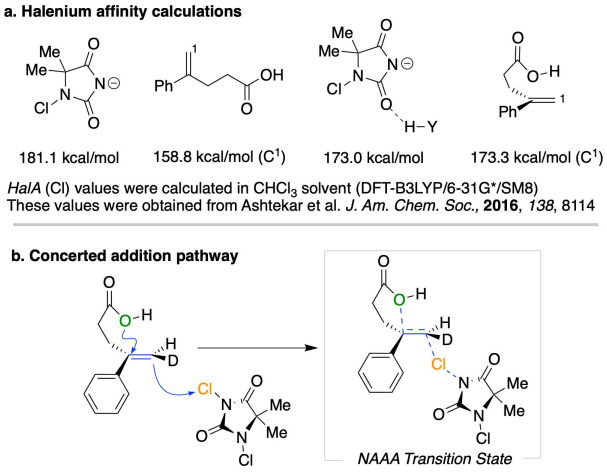

Figure 2. (a) Reported *HalA*(Cl) values; (b) Depiction of the concerted NAAA pathway for formation of *anti*-addition product.

enables "nucleophile assisted alkene activation" or NAAA, lowering the barrier for electrophilic attack on the alkene by raising the π HOMO energy and delocalizing the developing cationic charge (Figure 2b).[6]

To form the *syn*-chlorolactonization product above, we hypothesize a bimolecular NAAA transition state (TS), where the olefin is activated by the proximal oxygen to engage the chlorenium donor. Here, the DCDMH halenium donor is H-bonded to the carboxylic acid, concertedly transferring chlorine to the same alkene face (Figure 3) that bonds to the carboxylate oxygen. Recognizing that carboxylic acids are strongly dimerized in solvents such as chloroform, for the *anti*-TS, we revise the conceptual depiction in Figure 2 to envision a termolecular complex where the alkene's carboxylic acid moiety participates in H-bonding. This interaction promotes the carboxylate oxygen's nucleophilicity to activate the olefin, while an electrophilic chlorine (chlorenium ion) is delivered by DCDMH to the opposite face (Figure 3). The carboxylic acid's H-bonding partner could be another carboxylic acid, a non-reacting DCDMH molecule, or the MCDMH byproduct of the halogenating species. To characterize the *syn*- and *anti*-TSs, we explore here the factors that affect the stereochemical relationship between the chlorenium ion and the nucleophile (i.e. the *syn:*

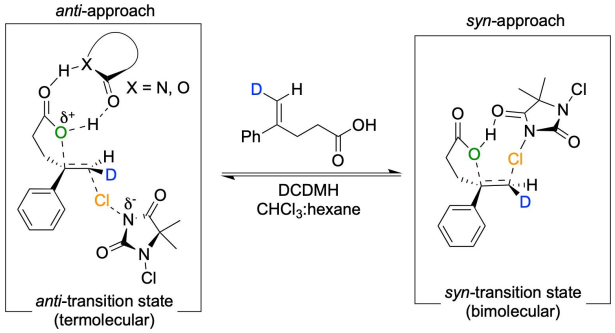

Figure 3. Transition states leading to *syn*- and *anti*-addition for chlorolactonization.

© 2024 The Author(s). Chemistry - A European Journal published by Wiley-VCH GmbH

anti ratio) as a function of (a) chlorenium ion donors, (b) solvent, (c) reactant concentrations, and (d) added components such as species that might participate as hydrogen bond partners in the TSs that ultimately lead to the *syn*- and *anti*-products.

To reveal the relative stereochemistry between the new sp^3 carbon centers formed by addition across the alkene, we synthesized **1-D**, the alkenoic acid substrate with a deuterium label in the terminal methylene. This deuterated substrate was accessed in a 4-step sequence: (a) silylation of alcohol **5**, (b) Pd-catalyzed deutero-hydroarylation,[7] (c) deprotection, and (d) oxidation (Scheme 2a). The deutero-hydroarylation afforded a high level of deuterium incorporation (88%) and good *Z:E* selectivity (95:5). The relative stereochemistry of addition could then be determined based on our earlier NMR assignments of the diastereotopic ^{1}H sites in the CHDCl group of the chlorolactone product (note that the stereochemistry of the deuterated substrate (*Z*) is the opposite of that originally employed (*E*) in our prior studies).[4] Specifically, carryover of the hydrogen from the starting alkene to the cyclization product reflects *syn* and *anti* additions, as shown in Scheme 2.

To probe the factors that determine *syn:anti* ratios in the uncatalyzed chlorocyclization of **1-D**, reaction conditions were systematically studied. First, chlorenium sources with a range of *HalA* values were evaluated (Table 1, entries 1–6) to explore whether this thermodynamically defined parameter affects the ease of electrophilic halogenation, modulating the *syn:anti* ratios.[6] The results indicate that variations in the chlorenium source do significantly impact the resulting *syn:anti* ratios, which range from 13:87 to 36:64. However, these variations do not appear to be simply correlated with *HalA*. Presumably, in the steps that lead to diastereoselectivity, the departing moieties of the chlorenium ion donors must be more directly involved than what is reflected in their simple *HalA* values.[8] In addition, as illustrated in Figure 3, the species participating in H-bonding with the carboxylic acid could be the original chlorenium ion donor or the byproduct of its reaction, each of which would vary as a function of reagent structure.

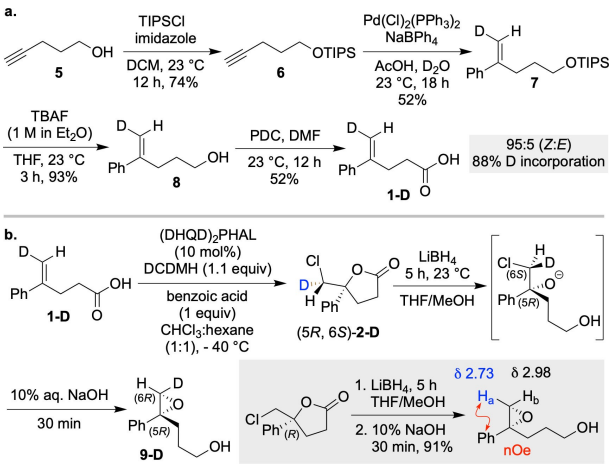

Scheme 2. (a) Synthesis of deuterated substrate **1-D**; (b) Absolute stereochemical assignment of the deuterated center (C6).

Next, the effects of solvents on *syn:anti* ratios were screened (Table 1, entries 7–11). In solvents with low polarity, such as toluene or dichloromethane, a higher amount of the *syn*-product was observed (56:44 and 45:55, respectively). This is in contrast to solvents with high polarity, such as acetonitrile, which afford increased *anti*-product (23:77 *syn:anti*). These solvent effects suggest mechanisms of different polarities for formation of the *anti*- and *syn*-chlorocyclization products. Increasing solvent polarity would be expected to stabilize the TS with more charge buildup and hydrogen bonding, consistent with the polarization of charge implied by the extended termolecular TS proposed for *anti* addition. Less polar solvents would be expected to favor the bimolecular concerted *syn* TS, in which little charge polarization occurs as it is balanced by proton transfer, concerted with chlorenium ion and oxygen addition across the alkene. An alternative interpretation suggested by a reviewer is that the more polar solvent inhibits the *syn* TS by disrupting hydrogen bonding of DCDMH with the substrate's carboxylic acid.

One striking deviation from the above noted trend is the surprisingly low *syn/anti* ratio seen when 1:1 v/v $CHCl_3$/Hexane is used as the reaction solvent (Entry 1 in Table 1). Based on a simple mole fraction-weighted average of the effective dielectric constant for this mixture, a greater proportion of *syn* product would be expected. However, entry 14, with essentially similar conditions and proportions, shows a very similar product ratio, indicating that this finding is not simply an erroneous outlier. These examples are, however, the only reactions run in mixed solvents, and it is possible that the two reaction paths, with their substantially different charge development, engage different solvent cages that differentially accelerate formation of *anti* product over *syn*.

These combined findings support the notion that two different mechanistic pathways are involved in formation of the *anti*- and *syn*-products, as depicted in Figure 3. For example, substantial charge separation is expected for the extended, termolecular TS leading to the *anti*-product, where one molecule of DCDMH delivers Cl^+ to a molecule of **1-D**, with a third species perhaps participating in a hydrogen bond relay that amplifies the adding oxygen site's nucleophilicity. This role could be fulfilled by the chlorenium donor (DCDMH), its dechlorinated byproduct (MCDMH), another molecule of **1-D**, or some other unidentified species. The resulting charge separation should be selectively supported by polar solvents, whereas lower medium polarity would favor the less polar bimolecular *syn*-forming TS (Figure 3).

Next, the effects of varying reagent concentrations were studied. Initially the concentration of the deuterated carboxylic acid **1-D** was kept constant while that of DCDMH was systematically varied (Table 1, entries 12–16). This 20-fold variation led to only a slight increase in *anti*-product at the highest DCDMH concentrations. This upturn could reflect a contribution from the higher DCDMH molecularity in the *anti* vs the *syn* TS. Next, the concentration of DCDMH was held constant while that of carboxylic acid **1-D** was systematically changed (Table 1, entries 17–19). These concentration changes also had little effect on the *syn:anti* ratio. When the concentrations of DCDMH

© 2024 The Author(s). Chemistry - A European Journal published by Wiley-VCH GmbH

Table 1. Screen of chlorinating reagents, solvents, and concentrations effect on *syn*:*anti* ratio of **1-D**.

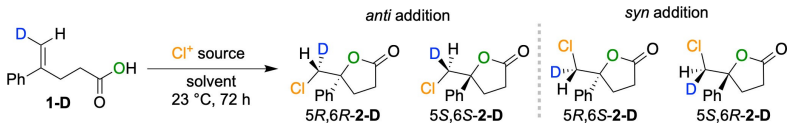

Entry	Cl^+ Source	*HalA* or Solvent ε	Solvent	[1-D] M	[Cl^+] M	*syn*:*anti*
1	DCDMH	275.7 (181.1)[a]	$CHCl_3$:Hex (1:1)	0.05	0.055	34:66
2	Di.Ch.T	273.3 (179.4)[a]	$CHCl_3$:Hex (1:1)	0.05	0.055	13:87
3	DCDPH	270.1 (178.1)[a]	$CHCl_3$:Hex (1:1)	0.05	0.055	36:64
4	NcSac	265.0 (171.7)[a]	$CHCl_3$:Hex (1:1)	0.05	0.055	21:79
5	TCCA	252.1 (161.0)[a]	$CHCl_3$:Hex (1:1)	0.05	0.055	22:78
6	CDSC	161.5 (149.6)[a]	$CHCl_3$:Hex (1:1)	0.05	0.055	25:75
7	DCDMH	37.5	CH_3CN	0.05	0.055	23:77
8	DCDMH	26.1	TFE	0.05	0.055	26:74
9	DCDMH	9.0	DCM	0.05	0.055	45:55
10	DCDMH	4.8	$CHCl_3$	0.05	0.055	49:51
(1)	DCDMH	3.7[b]	$CHCl_3$:Hex (1:1)	0.05	0.055	34:66
11	DCDMH	2.4	PhMe	0.05	0.055	56:44
12	DCDMH	-	$CHCl_3$:Hex (1:1)	0.05	0.0125	33:67
13	DCDMH	-	$CHCl_3$:Hex (1:1)	0.05	0.025	34:66
14	DCDMH	-	$CHCl_3$:Hex (1:1)	0.05	0.05	36:64
15	DCDMH	-	$CHCl_3$:Hex (1:1)	0.05	0.1	29:71
16	DCDMH	-	$CHCl_3$:Hex (1:1)	0.05	0.25	27:73
17	DCDMH	-	$CHCl_3$:Hex (1:1)	0.0125	0.05	27:73
18	DCDMH	-	$CHCl_3$:Hex (1:1)	0.025	0.05	28:72
(14)	DCDMH	-	$CHCl_3$:Hex (1:1)	0.05	0.05	36:64
19	DCDMH	-	$CHCl_3$:Hex (1:1)	0.1	0.05	33:67
(14)	DCDMH	-	$CHCl_3$:Hex (1:1)	0.05	0.05	36:64
20	DCDMH	-	$CHCl_3$:Hex (1:1)	0.025	0.025	41:59
21	DCDMH	-	$CHCl_3$:Hex (1:1)	0.0125	0.0125	52:48
22	DCDMH	-	$CHCl_3$:Hex (1:1)	0.00625	0.00625	54:46

[a] Numbers in parentheses represent *HalA* values that include simulated solvation energies for $CHCl_3$, as computed with the SM8 model on gas-phase optimized B3LYP/6-31G* geometries.[10] [b] The 1:1 v:v $CHCl_3$:hexane mixture has an estimated dielectric constant of 4.0, as calculated using the equation of Jouyban *et al.*[11] DCDMH = 1,3-dichloro-5,5-dimethylhydantoin, Di.Ch.T. = *N*,*N*-dichloro-p-sulfonamide, DCDPH = 1,3-dichloro-5,5-diphenylhydantoin, NcSac = N-chlorosaccharin, TCCA = trichloroisocyanuric acid, CDSC = chlorodiethylsulfonium hexachloroantimonate.

and substrate were both systematically decreased creating more dilute solutions of each reactant, *syn*-product formation increased (Table 1, entries 20–22) again consistent with *anti* product formation occurring via higher molecularity TSs. At lower concentrations, the proposed 1:1 complex of substrate: DCDMH would be favored (Figure 3) over the candidate termolecular proposed structures that lead to the *anti*-product. Thus, it is sensible that high dilution should favor formation of the *syn*-product.

With these data in hand, we conducted a more detailed kinetic investigation of the reaction to establish the order of the individual reactants in the rate-determining steps that respectively lead to the *syn* and *anti* addition products. As described by Bures, Variable Time Normalization Analysis (VTNA) uses graphical analysis of concentration vs time data, which is obtained from instances of the *same* reaction run with systematically different initial reactant concentrations.[9] Using NMR to monitor the reaction, we initially examined the original uncatalyzed conditions for chlorolactonization of **1-D** (Table 1, Entry 1), using $CDCl_3$ instead of $CHCl_3$ in a 1:1 chloroform: hexane solvent mixture. As noted above, *syn*- vs *anti*-addition products could be distinguished and quantified via integration of the diastereotopic hydrogen sites in the newly formed sp^3 carbon, CDHCl.[4] These analyses control mathematically for both the stereochemical purity and the unlabeled fraction of the substrate (see details for quantification and correction for unlabelled and minor isomeric form of **1-D** in the SI).

In the VTNA analyses, the concentration of each reactant, raised to a variable power, is used to adjust the time axis to enable direct visual overlaying of the results for different experiments. For each component, at least two experiments with different excess values of that component over another

© 2024 The Author(s). Chemistry - A European Journal published by Wiley-VCH GmbH

are needed, with all other conditions being held constant. By comparing the reaction profiles, these "different excess" experiments can reveal the order of the varied reactant.

For the present study, three different sets of conditions were studied, and the results were analyzed by VTNA (Table 2). Experiment B is the standard reaction conditions, using 0.05 M **1-D** and 0.055 M DCDMH. Experiment A has a lower concentration of **1-D**, 0.03 M with the DCDMH concentration held constant. Experiment C differs from B in raising the concentration of DCDMH to 0.10 M.

The NMR data enables simultaneous analyses of both *syn* and *anti* addition kinetics. The best overlay for the *syn*-addition, comparison of the reaction profiles of experiments A and B (different excess in carboxylic acid **1-D**) is obtained when the concentration of **1-D** is included with an exponent of 0.85 in the time axis, indicating that **1-D** is nearly first order with respect to formation of the *syn*-product (Figure 4a). Similarly, comparing reactions B and C, an exponent of 1.0 on [DCDMH] gives the best overlay, again pointing to first order behavior for *syn* product formation (Figure 4b). These findings combined with the results described above (concentration and solvent studies, Table 1) support the hypothesis of a bimolecular transition state for formation of the *syn*-cyclized product (Figure 3).

Table 2. Different experiments for VTNA studies.

Exp	1-D (M)	DCDMH (M)
A	0.03 M	0.055 M
B	0.05 M	0.055 M
C	0.05 M	0.10 M

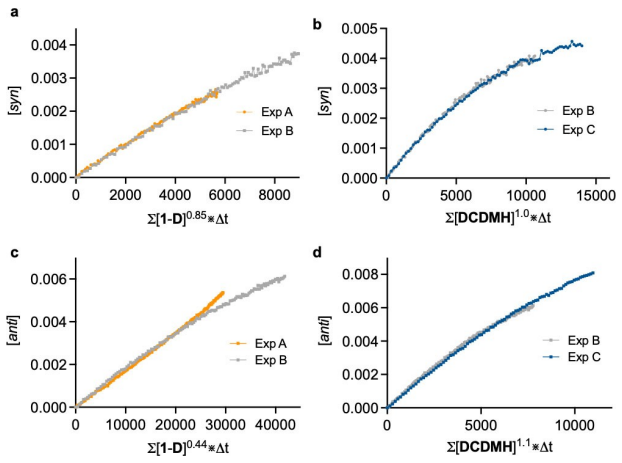

Figure 4. (a) VTNA analysis of **1-D** leading to the *syn*-product from a set of different excess experiments. The plots corresponding to experiments A and B overlay best when **1-D** is raised to the power of 0.85, indicating nearly *first order* dependence; (b) Similarly, experiments B and C show the best overlay when DCDMH is raised to the power of 1.0, indicating that DCDMH is also *first order*; (c) VTNA analysis of **1-D** leading to the *anti*-product from a set of different excess experiments. The plots from experiments A and B overlay best when [**1-D**] is raised to the power of 0.44, indicating *half order* dependence; (d) Plots from experiments B and C overlay best when [DCDMH] is raised to the power of 1.1, indicating a *first order* rate.

The VTNA analysis of the *anti*-addition finds that the carboxylic acid **1-D** shows the best overlay when raised to the order of 0.44 (Figure 4c), indicating that **1-D** has a *half order* dependance in forming *anti*-product. This finding might suggest a preequilibrium involving dimer formation of the carboxylic acid. Analysis of experiments B and C shows the best overlay upon raising DCDMH to the order of 1.1, indicating that DCDMH is *first order* with respect to formation of the *anti*-product (Figure 4d). It is important to note that unlike classical pseudo first-order kinetic studies, these reactions are run under synthetically relevant conditions (similar amounts of stoichiometrically related reagents). Exact integer order is not necessarily expected since these reactions can be affected by weak background associations, higher order molecularity, and/or averaging of different fragment orientations and transition state compositions for the overall reaction. Nonetheless, in this work the VTNA analyses of the rate data are substantially different for the *syn* vs *anti* cyclizations, implying differences in the corresponding transition states.

In VTNA plots combining the three experiments A–C, the reaction profiles should in principle become straight lines when each reactant's concentration is raised to the correct order, assuming no role for the reaction products.[9d] However, MCDMH, the byproduct of chlorenium ion donation from DCDMH, includes hydrogen bond-capable moieties like those in DCDMH and carboxylic acids, so we elected to explore its possible rate effects. As shown in Figure 5a, best overlays for *syn*-addition are found when [**1-D**] and [DCDMH] are included with near first order dependence (0.8 and 1.0, respectively), and zero order for MCDMH, indicating that MCDMH is not involved in the *syn*-addition. These data are consistent with the *syn*-cyclized product preferentially forming via the proposed bimolecular transition state (Figure 3). Similarly, when MCDMH was included in the analysis of *anti* product formation, it was found to have an order of 0.2, again suggesting little or no

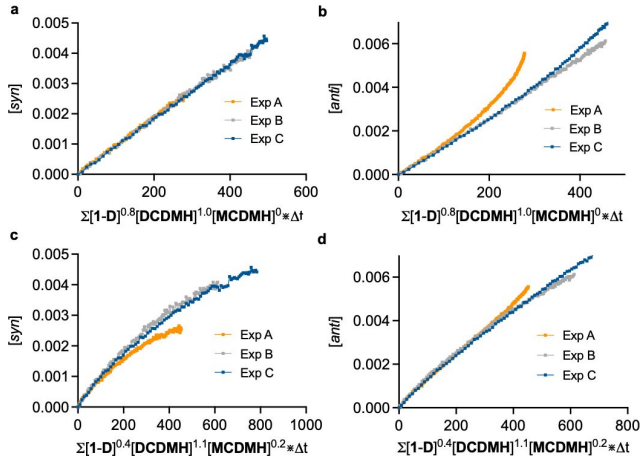

Figure 5. (a) VTNA overlay plots determining average reactant orders for alkene **1-D**, DCDMH, and MCDMH for *syn*-addition.; (b) VTNA plots of *anti*-addition product formation with component concentrations raised to the orders found for the *syn* reactions; (c) VTNA overlay of *syn*-addition products plotted with component concentrations raised to the orders found for the *anti* reactions; (d) VTNA plots determining average reactant orders for alkene **1-D**, DCDMH, and MCDMH for *anti*-addition.

© 2024 The Author(s). Chemistry - A European Journal published by Wiley-VCH GmbH

involvement (Figure 5d). As a check on the robustness of these visual analyses, the reaction orders found for *syn*-addition were applied to the *anti* data, (Figure 5b), and vice versa (Figure 5c). In both cases, the plots showed striking divergence, pointing firmly to distinct mechanisms for the two processes.

Interpretation of the results for the *anti*-transition state is more challenging. An overall reaction order of three would be expected for the proposed termolecular transition state (Figure 3) in which the carboxylic acid moiety participates in H-bonding to promote the oxygen (nucleophile) to activate the olefin, while a chlorine (electrophile) from DCDMH is transferred to the opposite face. However, the average reaction orders obtained from the VTNA studies find [**1-D**] at *half* order and DCDMH at *first* order, with a very small contribution from MCDMH. Half order kinetics for a given species is often interpreted to indicate that the component is in a pre-equilibrium with its dimer, which must dissociate to release reactive monomer.

The *anti* addition shows an overall reaction order of 0.2 for the MCDMH byproduct that forms as the reaction progresses; could this small fractional order reflect a contribution from MCDMH later in the process? To more thoroughly explore the possible role of MCDMH, we applied separate VTNA analyses to the initial and final phases of the reaction.[9b] In plots of experiments A, B, and C covering the initial third of the reaction, it was found that optimal overlay occurs when [**1-D**] is raised to the power 0.6, DCDMH is raised to 1, and MCDMH is raised to 0 (Figure 6a), consistent with the earlier findings of carboxylic acid at *half order*, DCDMH at *first order*, and MCDMH playing no role. However, the corresponding analysis from about the mid-point of the reactions shows a dependance on [MCDMH] (Figure 6b). Specifically, the plots overlay when the exponents for [**1-D**], [DCDMH], and [MCDMH] are 0.25, 1.1, and 0.6, respectively. Thus, as more of the reaction byproduct MCDMH builds up in the reaction mixture, it contributes more to promoting formation of the *anti*-cyclized product. Meanwhile, the alkene substrate itself appears to be moving toward a zero-order role.

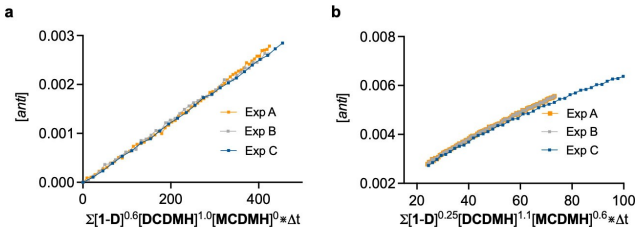

Figure 6. (a) VTNA analysis of experiments A, B, and C in the beginning of *anti*-product formation. These plots, which represent roughly 1/3 of the overall reaction (starting material consumption: Exp A, 0–47.1%; Exp B, 0–30.8%; Exp C, 0–32.5%), overlay when DCDMH is raised to 1, indicating *first order* participation, **1-D** is raised to 0.6 indicating *half order*, and MCDMH is raised to an order of 0.; (b) VTNA analysis of experiments A, B, and C at ~1/2 of the reaction path for *anti*-product formation (starting material consumption: Exp A, 47.1–96.9%; Exp B, 30.8–70.5%; Exp C, 32.5–91.9%). The plots overlay when the exponents for [DCDMH], [**1-D**], and MCDMH are 1.1, 0.3, and 0.7, respectively (data for experiment C truncated beyond 100 for clarity).

The above kinetic studies appear to point to the role of the hydrogen bond partner in the proposed termolecular transition state. This function could be fulfilled by multiple different species at different points in the reaction. The data from the VTNA studies suggest that the hydrogen bonding partner is primarily a second molecule of the carboxylic acid, but with a contribution from MCDMH as the latter grows in. Notably, quantum chemical analysis (*vide infra*) suggests that the hydrogen bond strength and oxygen polarization in an MCDMH-**1-D** heterodimer should be similar to that found in the homodimer of **1-D**.

Based on the VTNA results, MCDMH does show an effect on the rate of *anti*-cyclized product formation. To understand the role of MCDMH more accurately, concentration studies in the presence of MCDMH were performed (Table 3). Here, chloroform alone was used as the solvent as MCDMH is insoluble at higher concentrations in the mixed chloroform:hexanes solvent system. This insolubility highlights the hydrogen bonding abilities of MCDMH. A control reaction without MCDMH was also performed in chloroform to facilitate fair head-to-head comparisons (Table 3, entry 1).

At low concentrations, **1-D** and DCDMH showed a modest *syn* preference (69:31, *syn:anti*, Table 3, entry 1), consistent with the idea that the 1:1 complex would be favored at lower concentrations. Interestingly, when 0.1 M MCDMH was included, the selectivity switched to now favor the *anti*-product, with a *syn:anti* ratio of 38:62 (Table 3, entry 2). Sparked by these results, we evaluated another urea-type base, tetramethyl urea (TMU), that could not be chlorinated in the presence of DCDMH (Table 3, entry 3). The even stronger (11:89, *syn:anti*) preference for *anti* is consistent with hydrogen bonding by the urea to the carboxylic acid, enhancing its nucleophilicity in the termolecular transition state for *anti*-addition (Figure 3).

The small (0.2) value found for the average order of MCDMH in the *anti*-addition can be understood as follows: as [MCDMH] grows in, it may act as an additional H-bond relay partner for the three-component transition state. At low [MCDMH], we hypothesize that the carboxylic acid moiety of **1-D** is largely tied up in homodimers in the nonpolar medium. The dissocia-

Table 3. Effect of MCDMH and TMU[a] on the *syn*:*anti* ratio of **1-D**.

Entry	Solvent	[Sub]	[DCDMH]	[MCDMH]	[TMU]	*syn*:*anti*
1	$CHCl_3$	0.00625	0.00625	0	0	69:31
2	$CHCl_3$	0.00625	0.00625	0.1	0	38:62
3	$CHCl_3$	0.00625	0.00625	0	0.1	11:89

TMU = tetramethylurea.

© 2024 The Author(s). Chemistry - A European Journal published by Wiley-VCH GmbH

Table 4. Effect of benzoic acid on the *syn*:*anti* ratio of **2-D**.

Entry	Solvent	[Sub]	[DCDMH]	[benzoic acid]	*syn*:*anti*
1	$CHCl_3$:Hex (1:1)	0.05	0.055	0	36:64
2	$CHCl_3$:Hex (1:1)	0.05	0.055	0.05	27:73

tion equilibrium required for reaction is consistent with the VTNA finding of a *half order* dependance on [**1-D**]. To test this hypothesis, we added benzoic acid to the standard reaction (Table 4) which modestly increased the formation of the *anti*-product. This effect further suggests that the role of H-bond relay partner in the *anti*-transition state is fulfilled by either another copy of **1-D** or MCDMH. Based on our VTNA results, the dimer of alkene **1-D**, as well as MCDMH once produced, appears to act as the H-bond relay partner in the *anti*-addition transition state.

To summarize, the detailed VTNA analysis of the uncatalyzed chlorolactonization reaction leads to the following observations (See SI for experimental analysis and data):

a) The *syn*-addition shows first order dependence with respect to both the carboxylic acid **1-D** and the chlorenium ion donor DCDMH.
b) The *anti*-addition product shows first order dependence with respect to DCDMH, but an average half order dependence with respect to the carboxylic acid **1-D**. MCDMH shows involvement at increasing reaction order as the reaction progresses.
c) The two diastereomers arise from significantly different mechanisms.

Overall, VTNA and concentration studies have revealed the order of each reaction component for both *syn* and *anti* additions, providing evidence supporting their concerted transition states. Chlorine sources and solvents did not strongly modulate facial selectivity, but the observed variations as a function of chlorenium ion sources, solvents, reactant concentrations, and additives offered insights into the different concerted NAAA mechanisms at work for the two diastereomeric paths of chlorenium ion delivery and lactone ring closure.

Computational Analyses of Reaction Paths

To develop a more complete picture of the TS structures and reaction paths involved in the *syn*- and *anti*-chlorolactonizations discussed above, quantum chemical simulations were run using the B3LYP-D3 density functional[10a,12] with the 6-31G* basis set[13] using the Gaussian 16 quantum chemistry package.[14] After exploratory conformational searching, transition state structures for *syn* and *anti* attack paths were obtained and vibrationally characterized to verify their identities. To improve the estimate of energetics and account for the role of solvation in the chloroform reaction solvent, energies for these stationary points were recalculated at the B3LYP-D3/6-311++G** level, with solvation represented by the SMD polarizable continuum model of Cramer and Truhlar.[15] We designate this overall model B3LYP-D3/6-311++G**/SMD($CHCl_3$)//B3LYP-D3/6-31G*.

Combining the vibrational analyses and the higher-level electronic energies, free energy values were assigned to the respective structures, relative to their component fragments. From the located TSs, intrinsic reaction coordinate (IRC) calculations were pursued to verify their connections to the respective starting materials and products. In some cases, full IRC paths could not be completed, so simple optimizations were used to verify relaxation backward to starting materials and forward to the expected products.

Figure 7 illustrates the calculated paths for *syn* addition. Here, the main process is the transfer of the chlorenium ion from DCDMH to the methylene of the olefin, with concomitant closure of the lactone C–O bond. Two nearly isoenergetic TS (Figure 7a and b) structures were obtained for this process with the difference being the way the new C–O bond is formed. In one (Figure 7a) the attacking nucleophile is the carboxylate's -OH oxygen (in an 8-membered cyclic array of bonds), and in the other it is the carboxylate C=O oxygen (a 10-membered array). In this concerted reaction path, as positive charge builds up on the benzylic site, the carboxylate oxygen moves to form the C–O bond of the lactone product, while the hydantoin anion accepts the carboxylic acid proton, ultimately discharging that localized charge buildup. Interestingly, though intuition would suggest that the urea type carbonyl of the DCDMH should be the more basic site and therefore accept the proton, the lowest energy TSs found so far are the ones in which the amide-type carbonyl serves as the hydrogen bonding partner and proton acceptor. Overall, the computational results for the *syn* addition TS appear consistent with the experimentally observed first order kinetic behaviors of both chlorinating agent and substrate. Earlier work from our labs supported the concerted nature of this syn addition by ruling out the intermediacy of a benzylic carbocation based on kinetic isotope effects at the allylic C–H sites of the pentenoic acid substrate.[3,4]

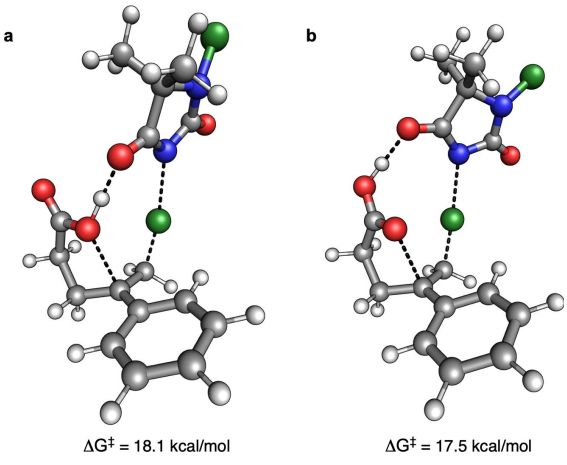

Figure 7. Concerted *syn* addition transition state structures where (a) carboxylate -OH and (b) carboxylate C=O oxygens serve as the nucleophilic partners, as computed at the B3LYP-D3/6-31G* level of theory. B3LYP-D3/6-311++G**/SMD($CHCl_3$)//B3LYP-D3/6-31G* free energies of activation relative to the separated fragments ($\triangle G^{\ddagger}$) are shown below.

© 2024 The Author(s). Chemistry - A European Journal published by Wiley-VCH GmbH

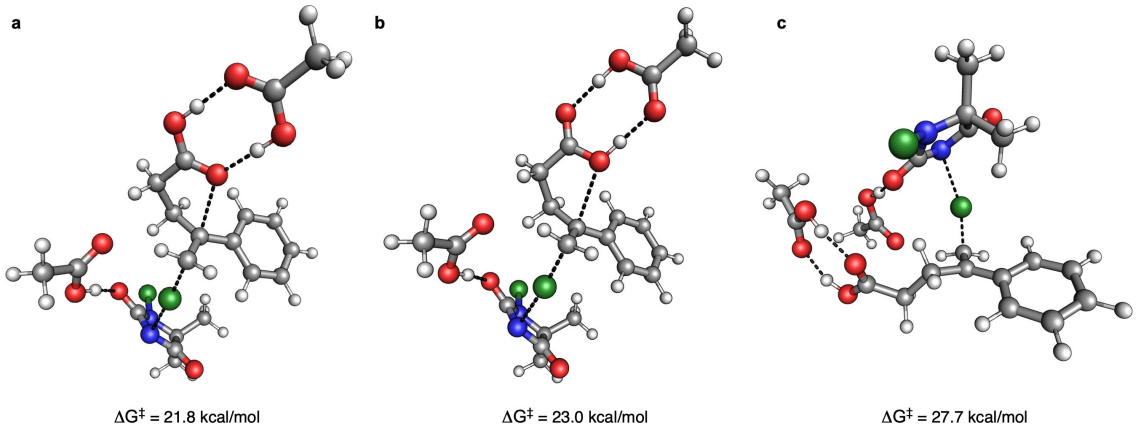

Figure 8. *Anti* TSs for (a) and (b) NAAA concerted and (c) stepwise chlorination paths considered for attack of DCDMH on substrate **1**. Relative B3LYP-D3/6-311 + +G**/SMD($CHCl_3$)//B3LYP-D3/6-31G* free energies for the three TSs are shown below. Note that the cation generated from TS (c) has little bias and could end up closing to either net *anti* or *syn* lactone products.

The *anti*-addition TSs and reaction paths are somewhat more complex than those for the *syn* case (Figure 8). Considered as a bimolecular process between substrate and DCDMH, the chlorolactonization would entail separation of charge, raising its energy cost substantially. In fact, simple attempts to model chlorenium ion transfer from DCDMH to substrate in an *anti* arrangement yields only paths that are monotonically uphill in energy. Even inclusion of the solvating effects of chloroform via the use of the SMD implicit solvation model as part of the optimizations is not sufficient alone to invert this trend; chlorenium transfer to the substrate's terminal alkene site is still uphill. However, noting the enhancement in *anti* product formation observed with the additives MCDMH, benzoic acid, and tetramethylurea, we explored possible ways in which these components could modify reactivity, serving as hydrogen bond partners to (a) the substrate's carboxylate moiety, stabilizing the positive charge that builds up there as the lactone ring closes, or (b) the DCDMH, stabilizing its buildup of negative charge as the chlorenium ion is transferred.

Success eluded our attempts to locate an *anti*-addition TS even when the system also included a carboxylic acid (here simulated as acetic acid) hydrogen bonded to the substrate's -COOH moiety. Additional activation at the chlorenium donor end was found to be necessary, in the form of carboxylic acid hydrogen-bonded to the DCDMH moiety. Given that simple carboxylic acids such as **1-D** would be expected to be substantially dimerized in chloroform solution, this need for an additional equivalent of undimerized acid is consistent with the half-order kinetics found for the alkenoic acid partner in the *anti*-additions.[16] Analogous structures in which it is the MCDMH byproduct that is hydrogen bonded to the reacting acid moiety and/or to the DCDMH were similarly located. Presumably, inclusion of hydrogen bonding to the DCDMH by these acidic partners enhances its electrophilicity as a chlorinating agent by stabilizing the negative charge buildup there. It might be expected that these more complex cluster complexes would be disfavored entropically and thus in free energy, but as noted above, no unstabilized TS structures for direct chlorenium delivery could be found, so it is clear that the potential energy stabilization outweighs the entropic costs of a more complex TS structure, as calculated at room temperature with the current model. Notable too is the computational finding that MCDMH is a stronger acid than simple carboxylic acids, which also enables this partner to function as an even more effective hydrogen bond donor to activate the DCDMH, consistent with the increase in molecularity observed for MCDMH's role in *anti* addition later in the reaction progress. Though the permutations and conformational possibilities of the various TS structures complexes are myriad, in Figure 8 we focus on the comparison between TS geometries in which the carboxylic acid dimer moiety is positioned over the alkene, participating in NAAA, vs. the more open geometry, which lies roughly 6 kcal/mol higher in free energy, presumably because the charge development at the benzylic position does not enjoy the additional delocalization of interaction with the carboxylate moiety.

It is informative to make internal comparisons within the *syn* and *anti* sets of computed TS structures. Thus, in the *anti* set, the concerted Ad_E3 path proceeds via a lower energy TS than the open cation. However, the fact that their respective compositions are so different (substrate + DCDMH for *syn*; substrate + DCDMH + 2 CH_3COOH for *anti*) and that the continuum solvation model is imperfect for strongly charge-separated species makes direct comparison of the ca. 18 (*syn*) vs ca. 22 (*anti*) kcal/mol computed $\triangle G^{\ddagger}$ essentially meaningless. In practice, the two paths must be effectively close enough in energy to deliver significant products for each, and the computed structures shown are more relevant to the issue of concerted vs stepwise reaction than to the relative proportions of *syn* vs *anti* cyclizations.

As an aside, in response to a reader's suggestion, we examined the possibility of the ene-like reaction in which the DCDMH reagent directly supplies the oxygen nucleophile, as well as the chlorine electrophile, as shown in Figure 9. This apparently promising scenario is found to have a computed barrier in excess of 30 kcal/mol, and so may be disregarded. Furthermore, given that relatively similar *syn* and *anti* results were experimentally obtained with other chlorenium ion donors, some of which completely lack a potential oxygen nucleophilic partner, we judge such a path to be unimportant.

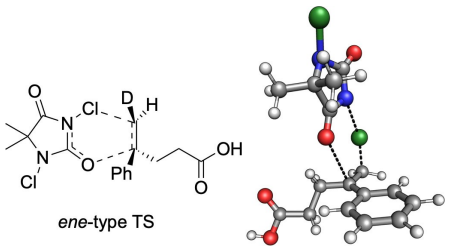

Figure 9. Alternative concerted chlorination path considered for DCDMH + **1-D** reaction. Such structures as calculated were found to be unrealistically high in energy.

© 2024 The Author(s). Chemistry - A European Journal published by Wiley-VCH GmbH

Conclusions

The rate-determining steps in the uncatalyzed chlorolactonization of 4-phenyl-4-pentenoic acid by DCDMH have been elucidated via kinetic analysis using VTNA, as well as through concentration, solvent, byproduct, and chlorine source studies. These findings indicate that MCDMH, the byproduct of DCDMH in the reaction, plays a significant role in the transition states for formation of both *syn* and *anti* products. These studies also determined that concerted delivery of the chlorenium ion to the nucleophile-activated olefin is a key feature in the transition states leading to the different selectivities, as illustrated by the computed reaction TSs in Figures 7 and 8. The intrinsic diastereoselectivities of chlorolactonization elucidated in this study illuminate the important features that drive selectivity for this transformation, and provide a key set of references for comparison to and guidance of catalytic stereochemical control in halofunctionalization reactions.

Acknowledgements

The authors are grateful for the generous support from the NSF (CHE-2154923).

Conflict of Interests

The authors declare no conflict of interest.

Data Availability Statement

The data that support the findings of this study are available in the supplementary material of this article.

Keywords: VTNA · Halogenation · Stereochemistry · Chlorolactonization · Deuterium labeling

[1] a) K. D. Ashtekar, A. Jaganathan, B. Borhan, D. C. Whitehead, Enantioselective Halofunctionalization of Alkenes. In *Organic Reactions*, John Wiley & Sons, **2021**, *Vol. 105*, pp. 1–266; b) Y. Cai, X. Liu, P. Zhou, X. Feng, *J. Org. Chem.* **2019**, *84*, 1–13; c) A. Castellanos, S. P. Fletcher, *Chem. Eur. J.* **2011**, *17*, 5766–5776; d) G. Chen, S. Ma, *Angew. Chem. Int. Ed.* **2010**, *49*, 8306–8308; e) Y. A. Cheng, W. Z. Yu, Y.-Y. Yeung, *Org. Biomolec. Chem.* **2014**, *12*, 2333–2343; f) S. E. Denmark, W. E. Kuester, M. T. Burk, *Angew. Chem. Int. Ed.* **2012**, *51*, 10938–10953; g) U. Hennecke, *Chem. Asian J.* **2012**, *7*, 456–465; h) M. L. Landry, N. Z. Burns, *Acc. Chem. Res.* **2018**, *51*, 1260–1271; i) K. Murai, H. Fujioka, *Heterocycles* **2013**, *87*, 763–805.

[2] a) D. C. Whitehead, R. Yousefi, A. Jaganathan, B. Borhan, *J. Am. Chem. Soc.* **2010**, *132*, 3298; b) R. Yousefi, D. C. Whitehead, J. M. Mueller, R. J. Staples, B. Borhan, *Org. Lett.* **2011**, *13*, 608–611.

[3] K. D. Ashtekar, M. Vetticatt, R. Yousefi, J. E. Jackson, B. Borhan, *J. Am. Chem. Soc.* **2016**, *138*, 8114–8119.

[4] R. Yousefi, K. D. Ashtekar, D. C. Whitehead, J. E. Jackson, B. Borhan, *J. Am. Chem. Soc.* **2013**, *135*, 14524–14527.

[5] R. Yousefi, A. Sarkar, K. D. Ashtekar, D. C. Whitehead, T. Kakeshpour, D. Holmes, P. Reed, J. E. Jackson, B. Borhan, *J. Am. Chem. Soc.* **2020**, *142*, 7179–7189.

[6] K. D. Ashtekar, N. S. Marzijarani, A. Jaganathan, D. Holmes, J. E. Jackson, B. Borhan, *J. Am. Chem. Soc.* **2014**, *136*, 13355–13362.

[7] H. X. Zeng, R. M. Hua, *J. Org. Chem.* **2008**, *73*, 558–562.

[8] N. S. Marzijarani, R. Yousefi, A. Jaganathan, K. D. Ashtekar, J. E. Jackson, B. Borhan, *Chem. Sci.* **2018**, *9*, 2898–2908.

[9] a) J. Burés, *Angew. Chem. Int. Ed.* **2016**, *55*, 2028–2031; b) J. Burés, *Angew. Chem. Int. Ed.* **2016**, *55*, 16084–16087; c) J. Burés, *Top. Catal.* **2017**, *60*, 631–633; d) C. D. T. Nielsen, J. Burés, *Chem. Sci.* **2019**, *10*, 348–353.

[10] a) A. D. Becke, *J. Chem. Phys.* **1993**, *98*, 5648–5652; b) A. V. Marenich, R. M. Olson, C. P. Kelly, C. J. Cramer, D. G. Truhlar, *J. Chem. Theory Comput.* **2007**, *3*, 2011–2033.

[11] A. Jouyban, V. Jouyban-Gharamaleki, M. Khoubnasabjafari, S. Soltanpour, W. E. Acree, *Phys. Chem. Liq.* **2022**, *60*, 910–921.

[12] a) S. Grimme, S. Ehrlich, L. Goerigk, *J. Comput. Chem.* **2011**, *32*, 1456–1465; b) P. J. Stephens, F. J. Devlin, C. F. Chabalowski, M. J. Frisch, *J. Phys. Chem.* **1994**, *98*, 11623–11627.

[13] a) R. Ditchfield, W. J. Hehre, J. A. Pople, *J. Chem. Phys.* **1971**, *54*, 724; b) P. C. Hariharan, J. A. Pople, *Theor. Chim. Acta* **1973**, *28*, 213–222; c) W. J. Hehre, R. Ditchfield, J. A. Pople, *J. Chem. Phys.* **1972**, *56*, 2257; d) A. D. McLean, G. S. Chandler, *J. Chem. Phys.* **1980**, *72*, 5639–5648.

[14] M. J. Frisch, G. W. Trucks, H. B. Schlegel, G. E. Scuseria, M. A. Robb, J. R. Cheeseman, G. Scalmani, V. Barone, G. A. Petersson, H. Nakatsuji, X. Li, M. Caricato, A. V. Marenich, J. Bloino, B. G. Janesko, R. Gomperts, B. Mennucci, H. P. Hratchian, J. V. Ortiz, A. F. Izmaylov, J. L. Sonnenberg, D. Williams-Young, F. Ding, F. Lipparini, F. Egidi, J. Goings, B. Peng, A. Petrone, T. Henderson, D. Ranasinghe, V. G. Zakrzewski, J. Gao, N. Rega, G. Zheng, W. Liang, M. Hada, M. Ehara, K. Toyota, R. Fukuda, J. Hasegawa, M. Ishida, T. Nakajima, Y. Honda, O. Kitao, H. Nakai, T. Vreven, K. Throssell, J. A. Montgomery Jr, J. E. Peralta, F. Ogliaro, M. J. Bearpark, J. J. Heyd, E. N. Brothers, K. N. Kudin, V. N. Staroverov, T. A. Keith, R. Kobayashi, J. Normand, K. Raghavachari, A. P. Rendell, J. C. Burant, S. S. Iyengar, J. Tomasi, M. Cossi, J. M. Millam, M. Klene, C. Adamo, R. Cammi, J. W. Ochterski, R. L. Martin, K. Morokuma, O. Farkas, J. B. Foresman, D. J. Fox, *Gaussian 16 Rev. C.01, Vol.*, Gaussian, Inc., Wallingford, CT **2016**.

[15] A. V. Marenich, C. J. Cramer, D. G. Truhlar, *J. Phys. Chem. B* **2009**, *113*, 6378–6396.

[16] Half-order reactions often occur in systems where a monomeric component is the active species, but the reagent is present mainly in unreactive dimer form. This behavior is common for carboxylic acids in organic solvents. For dimer A_2 dissociation to 2 monomers A, $K_{eq} = [A]^2/[A_2]$; the monomer concentration [A] available for reaction is therefore $= (K_{eq}[A_2])^{1/2}$. Thus, the concentration of free monomer available to react is proportional to [added reagent]$^{1/2}$. i.e. the square root of the concentration of added reagent..

Manuscript received: August 17, 2024
Accepted manuscript online: October 21, 2024
Version of record online: November 22, 2024

© 2024 The Author(s). Chemistry - A European Journal published by Wiley-VCH GmbH